Kinematical evolution of tidally limited star clusters: rotational properties

Maria A. Tiongco,[1][*] Enrico Vesperini[1] and Anna Lisa Varri[2]

[1]*Department of Astronomy, Indiana University, Bloomington, IN 47405, USA*
[2]*Institute for Astronomy, University of Edinburgh, Royal Observatory, Blackford Hill, Edinburgh EH9 3HJ, UK*

ABSTRACT

We present the results of a set of *N*-body simulations following the long-term evolution of the rotational properties of star cluster models evolving in the external tidal field of their host galaxy, after an initial phase of violent relaxation. The effects of two-body relaxation and escape of stars lead to a redistribution of the ordered kinetic energy from the inner to the outer regions, ultimately determining a progressive general loss of angular momentum; these effects are reflected in the overall decline of the rotation curve as the cluster evolves and loses stars. We show that all of our models share the same dependence of the remaining fraction of the initial rotation on the fraction of the initial mass lost. As the cluster evolves and loses part of its initial angular momentum, it becomes increasingly dominated by random motions, but even after several tens of relaxation times, and losing a significant fraction of its initial mass, a cluster can still be characterized by a non-negligible ratio of the rotational velocity to the velocity dispersion. This result is in qualitative agreement with the recently observed kinematical complexity that characterizes several Galactic globular clusters.

Key words: methods: numerical – globular clusters: general – galaxies: star clusters: general.

1 INTRODUCTION

The traditional picture of globular clusters is that they are spherically symmetric, isotropic and non-rotating stellar systems, a picture long supported by the success of spherical and isotropic equilibria such as King (1966) and Wilson (1975) models to fit the cluster surface density profiles (e.g. McLaughlin & van der Marel 2005; Miocchi et al. 2013). However, observational studies aimed at exploring the morphological and the kinematical properties of globular clusters are revealing a more complex picture showing deviations from spherical symmetry (see e.g. Chen & Chen 2010; see also the early pioneering study of White & Shawl 1987), and internal kinematics characterized by the presence of radial anisotropy (see e.g. Richer et al. 2013; Watkins et al. 2015; Bellini et al. 2015), and non-negligible rotation (see e.g. Meylan & Heggie 1997, and more recent works, including Lane et al. 2011; Bellazzini et al. 2012; Fabricius et al. 2014; Kacharov et al. 2014; Lardo et al. 2015; Cordero et al. 2017).

Observational studies have shown that the values of cluster rotational velocities normalized to the cluster central velocity dispersions range from about 0.05 to about 0.3 (see e.g. Bellazzini et al. 2012; Fabricius et al. 2014; Kacharov et al. 2014). Accurate radial profile measurements of the rotational velocities are in general not available for globular clusters, and the actual peak in the radial profile $V_{\rm rot}(r)/\sigma(r)$ could be larger than the values reported in existing observational studies, which are often based on measurements averaging the rotational velocities over a broad range of cluster-centric distances. Moreover line-of-sight observations provide information on projected velocities and do not allow a direct determination of the actual $V_{\rm rot}/\sigma$.

It is also important to emphasize that the present-day rotation in globular clusters is likely to be the remnant of a stronger early rotation weakened by the effects of two-body relaxation (see Mapelli 2017 for an example of hydrodynamical simulations producing rotating young massive clusters and Hénault-Brunet et al. 2012 for measurements of rotation in young massive cluster R136); specifically, during the cluster long-term evolution, the magnitude of the rotation decreases due to escaping stars carrying away angular momentum, and the angular momentum of the remaining stars being redistributed on the relaxation time-scale (see e.g. Akiyama & Sugimoto 1989; Einsel & Spurzem 1999; Kim et al. 2002; Kim, Lee & Spurzem 2004; Ernst et al. 2007; Kim et al. 2008; Hong et al. 2013). The results of these pioneering theoretical works have shown that rotation can affect several important aspects of cluster evolution such as core collapse and the mass-loss rate.

The neglect of rotation in the study of globular cluster dynamics does not appear to be justified either by theoretical or by observational studies, and as we enter the *Gaia* era and new results from European Southern Observatory/Very Large Telescope and *Hubble Space Telescope* studies are sharpening the dynamical picture of clusters, a renewed effort to further our understanding of the role of internal rotation and its evolution in globular clusters is necessary.

---

[*] E-mail: mtiongco@indiana.edu

In this paper, we present the results of a set of *N*-body simulations following the long-term evolution of tidally limited models of star clusters, as initially resulting from an early phase of violent relaxation in the presence of an external tidal field. The focus of this study is on the evolution of the angular momentum content, by means of a complete characterization of the rotational properties of the systems under consideration. We will devote particular attention to the dynamical interplay between the internal rotation and the effects of the tidal field of the host galaxy, with the goal of investigating the connection between the evolution of the angular momentum and the different stages of cluster evolution.

The outline of this paper is as follows: In Section 2, we describe our method and the initial conditions adopted. We present our results in Section 3 with a general discussion of the evolution of the rotation curve along with a discussion focused on some specific features such as the peak of the rotation curve and the strength of rotation in the cluster inner and outermost regions. Finally, in Section 4, we summarize our conclusions.

2 METHOD AND INITIAL CONDITIONS

The *N*-body models featured in this paper were originally presented in Tiongco, Vesperini & Varri (2016a), in the context of a study of the long-term evolution of the velocity anisotropy of tidally limited star clusters. The simulations follow the evolution of systems that first undergo violent relaxation in the host galaxy tidal field, modelled as a point mass. The clusters are assumed to be on circular orbits, and equations of motions are solved in a reference frame corotating with the cluster around the host galaxy centre (see e.g. Heggie & Hut 2003), with angular velocity Ω. Particles are removed from the simulation once they move beyond two times the Jacobi radius, r_J. We carry out our simulations using the NBODY6 code (Aarseth 2003) accelerated by a GPU (Nitadori & Aarseth 2012) on the BIG RED II cluster at Indiana University.

For the initial violent relaxation phase, we use different initial values of the virial ratio, $Q = T/|V|$ (where *T* and *V* are the system kinetic energy and potential energy, respectively), and different ratios of the initial cluster limiting radius (the radius measuring the total initial size of the cluster) to the Jacobi radius (the limit on the cluster size imposed by the external tidal field of the cluster host galaxy; see e.g. Heggie & Hut 2003), r_L/r_J. We use the following parameters for the initial conditions of the violent relaxation phase: (Model ID, Q, r_L/r_J): (vrQ01F05, 0.1, 0.5), (vrQ01F02, 0.1, 0.2) and (vrQ001F05, 0.01, 0.5). The systems are initially spherical, homogeneous and have equal-mass particles, beginning with a slightly larger number of particles in order to take into account the loss of stars in the violent relaxation phase.

Vesperini et al. (2014) characterized in detail the kinematical properties that emerge from the violent relaxation process under the influence of the tidal field and the effects of the Coriolis force on the stars' orbits. We refer to that paper for further details on the early evolution of kinematical properties; for the purposes of this paper, the main kinematical feature of these models is that they are characterized by differential rotation around an axis perpendicular to the orbital plane. In the frame of reference corotating with the cluster, the rotation is prograde in the inner regions and retrograde in the cluster outermost regions; more specifically, the rotation curve increases from the cluster centre, peaks at a distance from the cluster centre equal to approximately the half-mass radius, and then decreases to a retrograde rotation in the outermost regions. The black lines in the top panels of Fig. 1 show the rotational velocity radial profiles emerging at the end of the violent relaxation phase

as measured in the corotating frame of reference (the rotational velocity measured in the non-rotating coordinate system is shown in the bottom panels of Fig. 1).

In this paper, we focus on the subsequent *long-term* evolution of the rotational properties of these systems. From here onward, we mark the time at the end of the violent relaxation phase (when the large-scale structural oscillations associated with the initial virialization process end, typically after a few dynamical times; see Vesperini et al. 2014) as our initial time, $t = 0$. We measure the essential properties of the systems (such as the number of particles and the ratio of the half-mass radius to the Jacobi radius) at this time, and we refer to these properties as the initial conditions of the long-term evolution. We list these properties in Table 1, and note that for each model, these values are the averages obtained from four different simulations following the evolution of different random realizations of the same model. When we show the time evolution of the cluster rotational properties, time is normalized to the cluster initial relaxation time $t_{rh,i} = 0.138 N^{1/2} r_h^{3/2}/(\langle m \rangle^{1/2} G^{1/2} \log(0.11N))$, where *N* is the number of stars, $\langle m \rangle$ is the star mean mass and r_h is the 3D half-mass radius (see e.g. Spitzer 1987). For a cluster with, for example, $\langle m \rangle = 0.6\,M_\odot$, $N = 2 \times 10^5$ and $r_h = 3$ pc, $t_{rh,i} \sim 600$ Myr. All the simulations are run until 75 per cent of the mass they had at the end of violent relaxation is lost.

3 RESULTS

3.1 Evolution of the rotation curve

We start our analysis by considering the time evolution of the rotation curves of our three models. In Figs 1–3, we plot the rotational velocity (v_ϕ, as measured about the *z*-axis) for each of the models versus the projected radius *R* normalized to the projected half-mass radius, R_h. We normalize v_ϕ in a few different ways: to the rotation speed of the coordinate system at the initial Jacobi radius ($\Omega r_{J,i}$, Fig. 1), to the averaged velocity dispersion $\sigma = \sqrt{\frac{1}{3}(\sigma_r^2 + \sigma_\phi^2 + \sigma_\theta^2)}$ in cylindrical bins measured at *R* (Fig. 2) and to the central velocity dispersion as sometimes done in observational studies (Fig. 3). We define the central velocity dispersion as the velocity dispersion of the innermost 500 stars in the system.

The profiles are constructed by combining five snapshots around the desired time, taking into consideration all particles within the Jacobi radius and binning them in cylindrical shells with heights encompassing the entire cluster. All desired quantities are measured in each bin, and this process is repeated for each of the four realizations. Then at each radius *R*, the median value of all the realizations is taken to create the profiles shown in Figs 1–3.

The strength of the initial rotation in the three models is determined by the initial conditions of the violent relaxation phase: Systems with a colder initial virial ratio or higher initial r_L/r_J develop stronger rotation (see Vesperini et al. 2014 for further details). The three models, although characterized by different strengths of the initial rotation, share a number of common features in the evolutionary path of their rotational velocity radial profiles:

(i) For all models, rotation becomes weaker as the system evolves and loses mass; as pointed out in the Introduction section, this implies that the rotation observed in clusters today is just the remnant of a stronger initial rotation, and a weak present-day rotation cannot be used to rule out the importance of rotation for the cluster dynamical history.

(ii) A non-negligible rotation is retained for a large fraction of the cluster life; for example, the vrQ001F05 model is still characterized
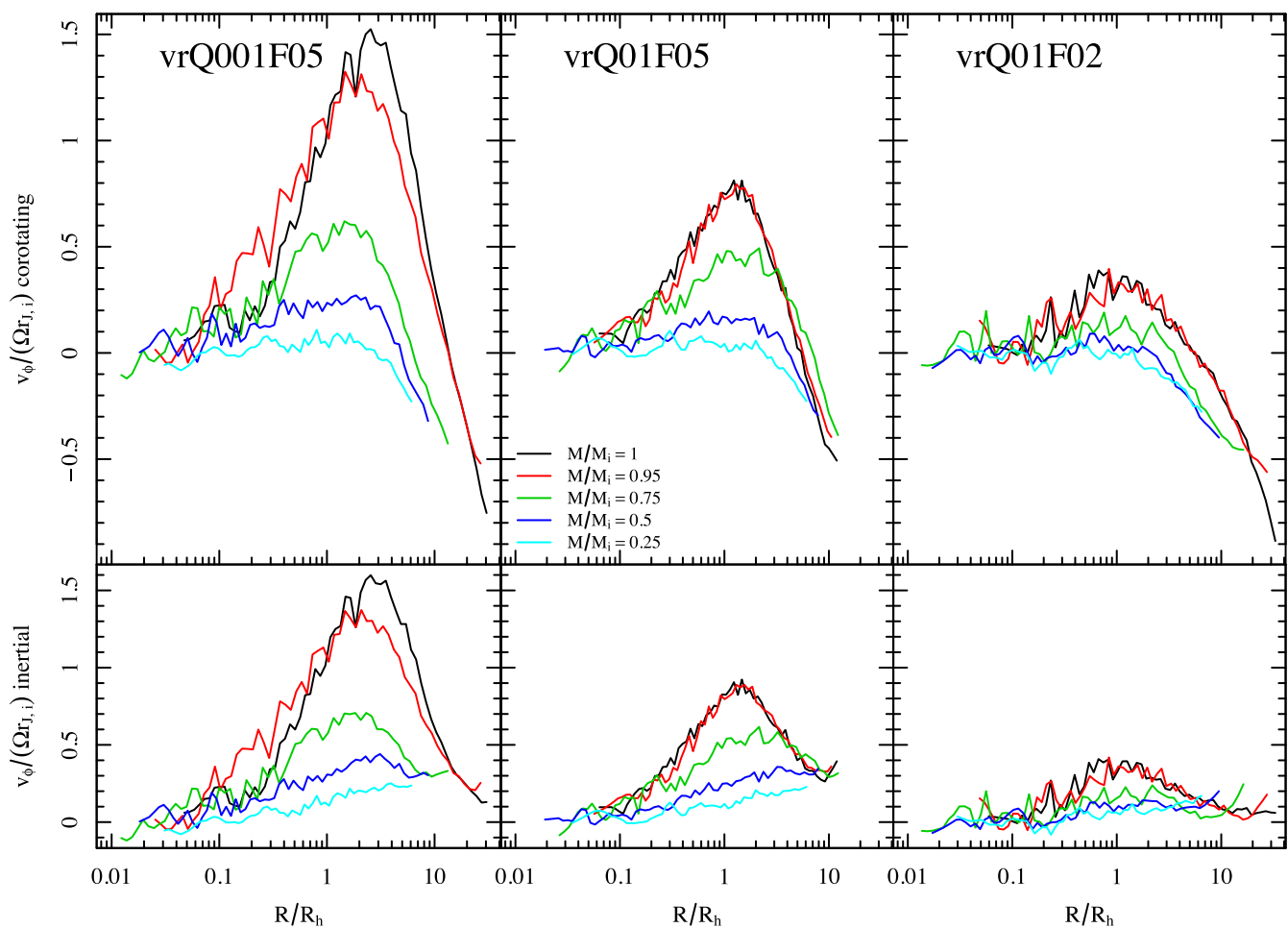
Figure 1. Evolution of the rotation curves for all the models. Each coloured line represents the system at different times chosen when the system contains a certain fraction of its initial mass, M/M_i. In the construction of the profiles, all particles within the Jacobi radius have been considered. Top panels: the v_ϕ component of the velocity normalized to the rotation speed of the coordinate system at the initial Jacobi radius, $\Omega r_{J,i}$, in the corotating reference frame. Bottom panels: the same profiles in the non-rotating, i.e. inertial reference frame.

Table 1. Summary of simulations.

Model ID	$N_{i, avg}$	$(r_h/r_J)_{i, avg}$	Realizations
vrQ01F05	14 860	0.095	4
vrQ01F02	16 287	0.036	4
vrQ001F05	17 091	0.036	4

by a peak v_ϕ/σ equal to about 0.35 after losing 25 per cent of its initial mass (see Fig. 2, top left-hand panel) and the model vrQ01F05 has a peak v_ϕ/σ equal to about 0.3 after losing 25 per cent of its initial mass (see Fig. 2, top middle panel).

(iii) The value of the peak in the profiles of v_ϕ/σ and v_ϕ/σ_0 decreases as the cluster evolves and loses mass, but its location within the cluster is approximately constant during the entire cluster evolution and found at about 1–2R_h.

(iv) All models are initially characterized by an inner prograde rotation and outer retrograde rotation. As the cluster evolves, the inner prograde rotation is gradually erased. The outer retrograde rotation emerging at the end of the initial violent relaxation, as a result of the symmetry breaking introduced by the external tidal field in the collapse phase and of the effects of the Coriolis force on the orbit of the stars (see Vesperini et al. 2014), persists for all models for the entire evolution of the cluster, due to the subsequent interplay

between the evolution of the fraction of prograde and retrograde stars and the effects of the tidal field (see Tiongco, Vesperini & Varri 2016b).

In the following sections, we discuss in further detail the evolution of the main features of the rotation curves of our models.

3.2 Evolution of the peak of the rotation curve

Though in the previous section we characterized the evolution of rotation throughout the system, observationally, such a complete characterization of the rotational velocity profile is extremely difficult. A well-established method to measure the rotation in a cluster is through spectroscopy and line-of-sight radial velocity measurements of a sample of stars; the samples in current studies can reach up to a few hundred stars, and although they rarely span a range of radial distances broad enough to construct a complete rotation curve (see e.g. Bianchini et al. 2013; Kacharov et al. 2014; Cordero et al. 2017 for some recent studies of the rotational properties of selected Galactic globular clusters), they can be sufficient to identify the peak of the rotation curve.

In the previous section, we have shown that the magnitude of the peak of the rotation curve decreases with time and that its distance from the cluster centre relative to the cluster half-mass radius
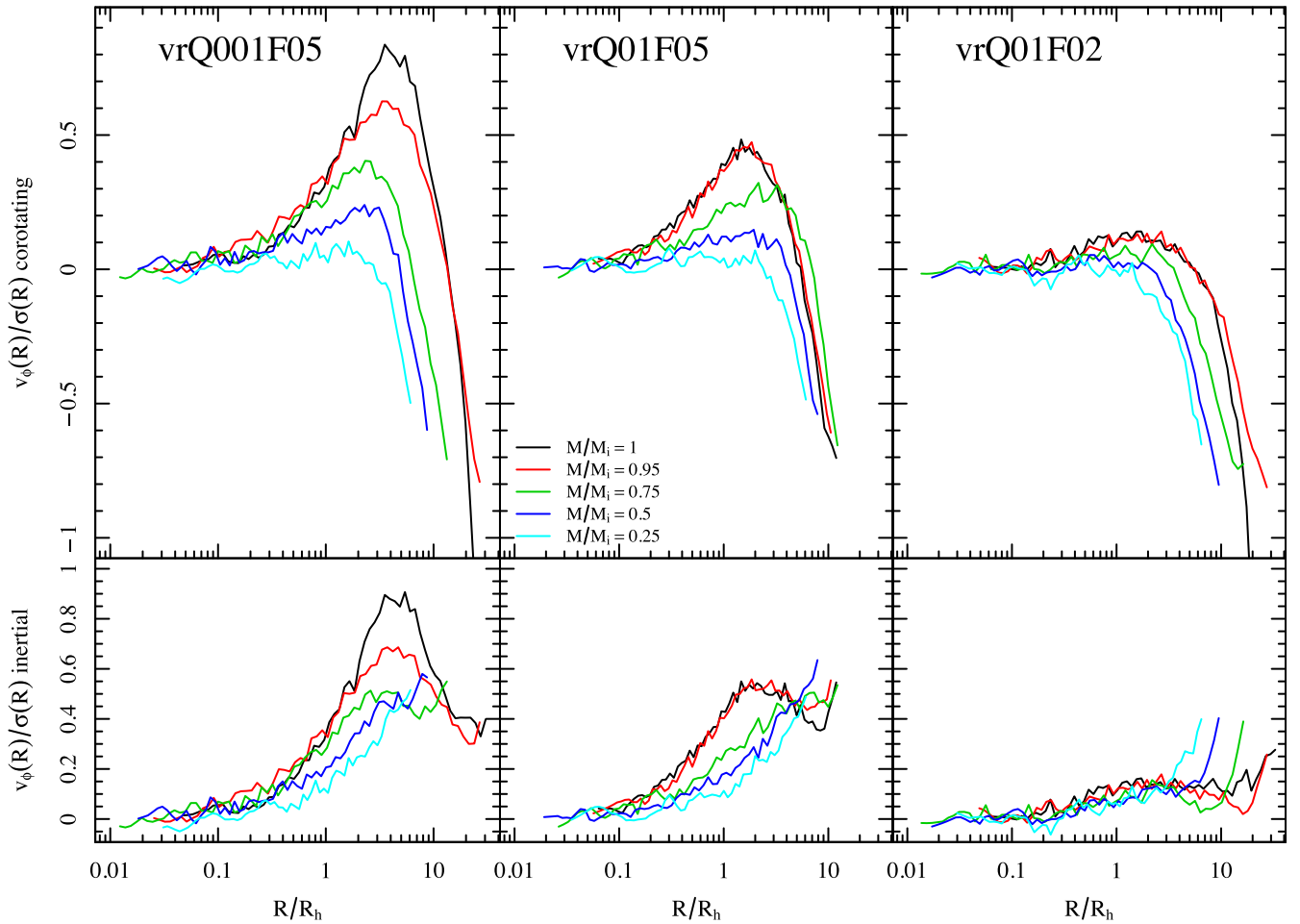
Figure 2. Time evolution of the rotational velocity profile divided by the velocity dispersion profile. See Fig. 1 for further details about the adopted colour scheme and organization of the panels.

remains approximately constant around $1-2R_\mathrm{h}$. In Fig. 4, we take a closer look at the time evolution of the magnitude of the peak of the rotation curve, v_pk. Fig. 4 shows that although v_pk immediately starts to decrease, its rate of decrease undergoes a transition at the time of core collapse when v_pk starts to decrease significantly more rapidly; we interpret this transition in the time evolution of v_pk as the consequence of the onset of the post-core-collapse expansion. The subsequent evolution is characterized by a gradual slowdown in the decrease rate of v_pk, allowing the cluster to retain a non-negligible value of v_pk after several tens of initial half-mass relaxation times.

In Fig. 5, we show the evolution of v_pk, this time normalized to the initial value of v_pk, as a function of the fraction of the initial mass remaining in a cluster; as discussed in the Introduction section, the combined effect of angular momentum transport from the inner to the outer regions and star escape results in the overall loss of angular momentum, and thus contributes to the decline in the strength of rotation. Fig. 5 shows that the systems we have studied almost universally lose the same fraction of their initial rotation for the same amount of mass lost, and even after losing about 50–60 per cent of their initial mass, they still retain some of their initial rotation.

As for the location of the peak, R_pk, Fig. 6 shows that the peak location relative to the half-mass radius begins near $1-2R_\mathrm{h}$ for all of the models, then moves slightly inward over time. This likely reflects the post-core-collapse expansion of the half-mass radius,

while the cluster itself is decreasing in size as it loses stars and the Jacobi radius moves inward.

Next, we look at the evolution of v_pk/σ_0 as a function of time [Fig. 7, where we also show the evolution of the peak of the $v_\phi(R)/\sigma(R)$ profile], and normalized to its initial value versus the fraction of initial mass remaining (Fig. 8). This normalization using the central velocity dispersion is often adopted in the literature because of the lack of observational measurements of the full radial profile of the velocity dispersion.

Fig. 7 clearly illustrates how the ratio of the rotational velocity to the velocity dispersion, and therefore the estimate of the relative importance of ordered and random motions in a cluster, depends on which value of the velocity dispersion is used for the normalization. It is interesting to point out how these figures show that clusters can retain values of v_pk/σ_0 similar to those found in observational studies (see the initial discussion in the Introduction section) after several tens of initial relaxation times and after having lost a significant fraction of their initial mass. Fig. 8 shows a similar trend to Fig. 5, where the systems almost universally lose the same fraction of their initial v_pk/σ_0 for the same amount of mass lost [we also observe a similar trend for the fraction of initial peak value of $v_\phi(R)/\sigma(R)$ versus mass lost].

The time evolution in Fig. 7 is due to the combined effect of the evolution of v_ϕ and σ; it is interesting to point out that, similarly to what was already found in Fig. 4, the rate of evolution of v_pk/σ_0
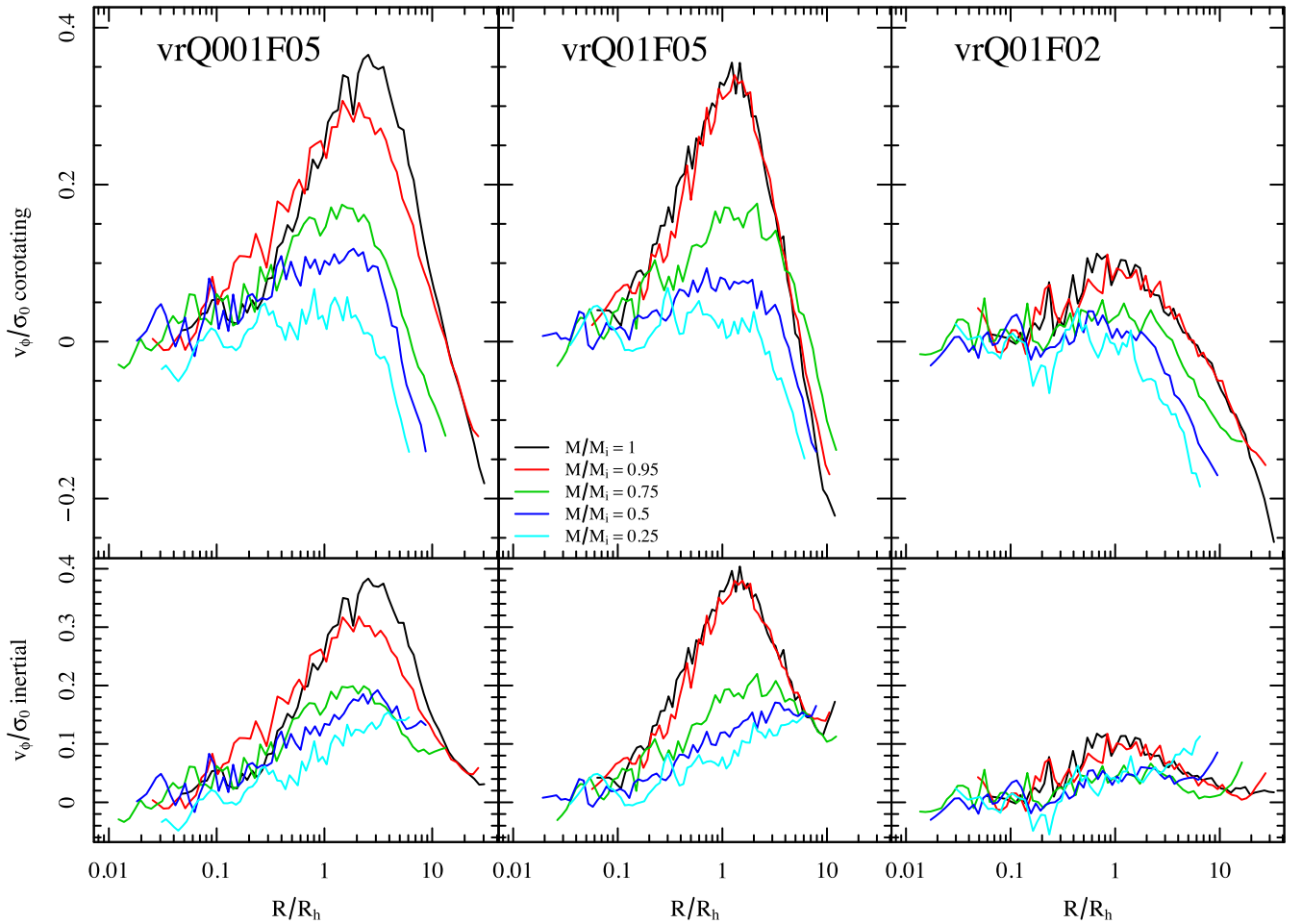
Figure 3. Time evolution of the rotational velocity profile divided by the central velocity dispersion. See Fig. 1 for further details about the adopted colour scheme and organization of the panels.

appears to undergo a sharp transition to slower rates after core collapse (at about 15 $t_{\rm rh, i}$); we interpret this as the result of the decrease in velocity dispersion associated with the post-core-collapse expansion (see e.g. Giersz & Heggie 1994).

Finally, in Fig 9, we show the evolution of the magnitude of the rotation peak in the different forms calculated above as a function of its location within the cluster. The models appear to fall along a universal line (although with some significant noise) and follow a trend that further illustrates the evolution towards smaller values of the rotation peak at radii slightly closer to the cluster centre.

3.3 Evolution of the slope of the rotation curve in the inner regions

A number of observational studies have provided a measure of the rotation of the cluster inner regions. In particular, in a recent study, Fabricius et al. (2014) have used data acquired with an Integral Field Unit (IFU) spectrograph to measure rotation in the central regions of 11 Galactic globular clusters. Although these data provide only an approximate global measurement of the rotational properties of the central and intermediate regions of the clusters and do not shed light on the details of the rotational velocity radial profile, they are never the less an important addition to the study of cluster kinematics and have provided further evidence of the presence of

non-negligible rotation in globular clusters, even when they are in a relatively advanced stage of their dynamical evolution.

In this section, we focus our attention on the cluster inner rotation; in order to quantify the strength of a cluster inner rotation, we have measured the slope of the inner rotation curve by using both a linear fit of the inner rotation curve and the method employed by Fabricius et al. (2014). The latter method involves fitting a 2D function to the radial velocity field of the cluster inner regions: The gradient of this function provides a measure of the slope of the inner rotation that, in the case of solid-body rotation, coincides with the cluster angular velocity. We refer to the measured slope as $\omega_{\rm in}$ and normalize it to the angular velocity of the cluster orbital motion around the host galaxy, Ω. For our calculation, we have used particles between 0.1 and $0.5 R_{\rm h}$, combining five snapshots around the desired time with, typically, ~4000 particles per snapshot at the beginning and ~1000 particles per snapshot at the end of the simulation, and for the calculation based on the method adopted in Fabricius et al. (2014), we have used the radial velocities measured along a line of sight perpendicular to the rotation axis.

Figs 10 and 11 show the evolution of $\omega_{\rm in}/\Omega$, found using the linear-fitting method, respectively, as a function of the time normalized to the initial half-mass relaxation time and then normalized to its initial value as a function of the fraction of the initial mass remaining in the cluster. In this and the following sections, profiles were calculated individually for each realization, and the median
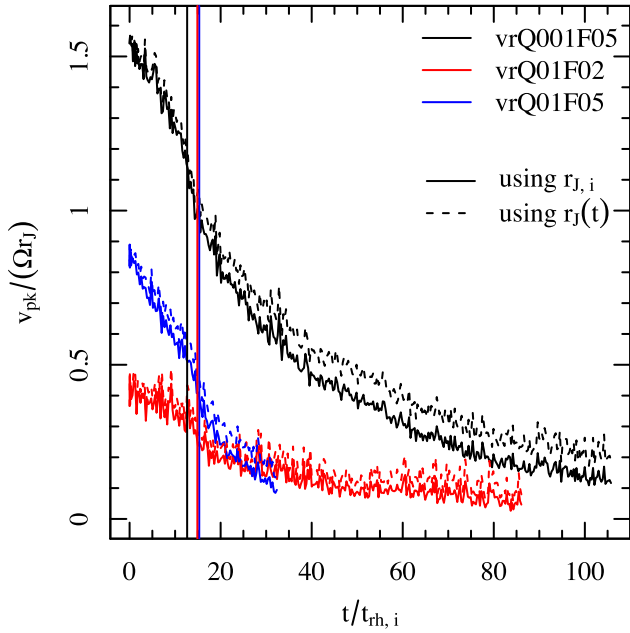
Figure 4. Evolution of the magnitude of the peak of the rotation curve for all the models as a function of time. The two differing line types distinguish between normalizing with the initial Jacobi radius or the one at that time. The vertical lines mark the time of core collapse, calculated as the median of the values obtained in the different model realizations.
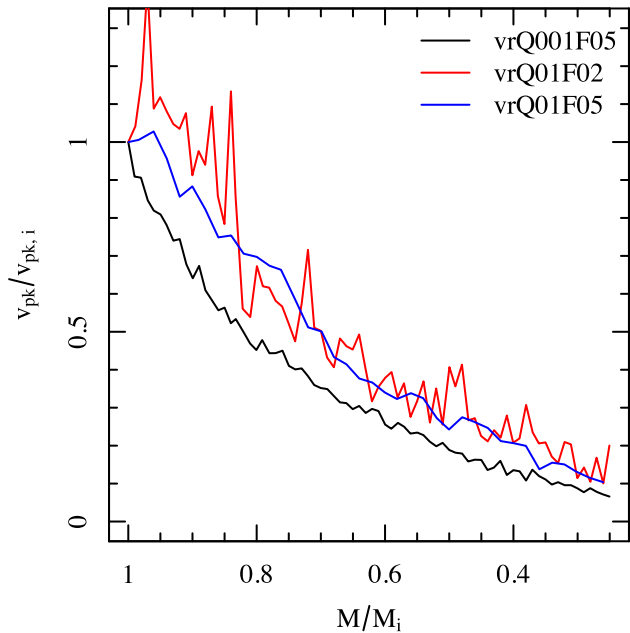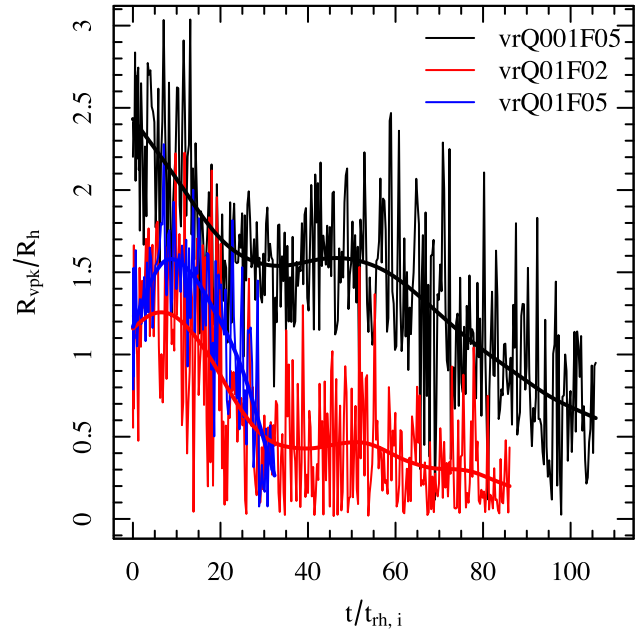

Figure 6. Evolution of the location of the peak of the rotation curve for all the models as a function of time. The thicker lines are a smoothing spline fit added to guide the eye.
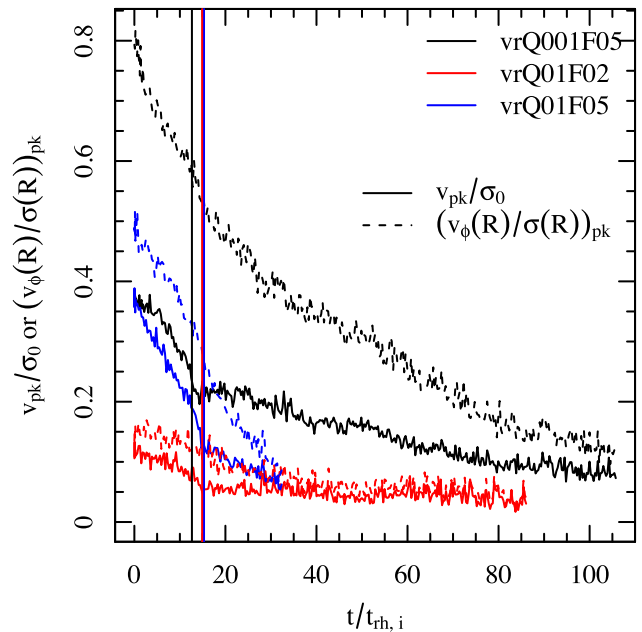

Figure 5. Evolution of the magnitude of the peak of the rotation curve normalized to its initial value as a function of fraction of initial mass remaining in the cluster.

Figure 7. Evolution of the magnitude of the peak of the rotation curve normalized to the velocity dispersion for all the models as a function of time. The two differing line types distinguish between v_{pk}/σ_0 and the peak of the v_ϕ/σ profile. The vertical lines mark the time of core collapse.

values of ω_{in}/Ω from each profile are plotted as the solid lines in these figures. The shaded areas around each line represent the range covered by the four realizations of each model.

All the simulations are characterized by a decline in the inner rotation as the system evolves. We point out, however, a notable feature in the time evolution of ω_{in}/Ω for the simulation vrQ001F05: In this model, ω_{in}/Ω slightly increases during the early phases of the cluster evolution (for $t < 5t_{rh, i}$). We interpret this increase as a

manifestation of the gravogyro instability, a phenomenon in which angular momentum being transported outward causes the cluster to contract due to lack of centrifugal force and thus increases the angular speed near the centre of the cluster (see Inagaki & Hachisu 1978 for the first theoretical investigation of this process in the context of fluid cylindrical shells, and Akiyama & Sugimoto 1989 and Ernst et al. 2007 for further discussion of this process, as an application to the interpretation of the evolution of N-body models with initial
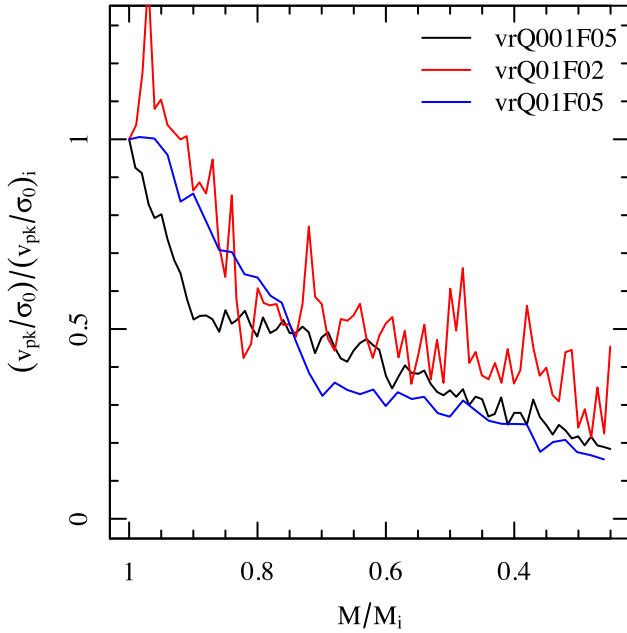
Figure 8. Evolution of the magnitude of v_{pk}/σ_0, normalized to its initial value as a function of the fraction of the initial mass remaining in the cluster.

rotation). Similar to what was discussed in the previous sections, the evolution of the inner angular velocity also appears to undergo a transition at the time of core collapse around $t \sim 15t_{rh,\,i}$. We emphasize that the inner rotation, although also undergoing a significant decrease during the cluster evolution, is still non-negligible after several tens of initial half-mass relaxation times and after the cluster has lost a large fraction of its initial mass. At the end of our simulations, $\omega_{in}/\Omega \sim 1$–$2$; many real clusters are likely to be in a less advanced stage of their evolution and should therefore be characterized by larger values of this ratio.[1]

Finally, in Fig. 12, we compare the values of ω_{in}/Ω for the simulation vrQ001F05 obtained with the two different methods described above, and we find them to be consistent with each other. This further reinforces the potential for IFU data to greatly complement results from spectroscopic surveys focusing on individual stars.

We conclude this section by pointing out that clusters starting with any of the initial conditions we have considered and currently at a similar evolutionary stage will be characterized by similar values of ω_{in}/Ω; for clusters at different galactocentric distances, R_g, in a galaxy like the Milky Way with a flat rotation curve ($\Omega \propto 1/R_g$), this would result in a trend of ω_{in} decreasing with R_g. A dispersion around this relation could arise as a result of a combination of effects due to differences in the initial cluster properties, in the cluster dynamical ages, and in the angle between the line of sight and the rotation axis. Interestingly, the results of the observational study of Fabricius et al. (2014) show some evidence of such a broad trend between inner angular velocity and galactocentric distance.

3.4 Evolution of the rotation in the outermost regions

In Tiongco et al. (2016b), we showed that, as a result of the co-operation between the preferential loss of stars on prograde orbits

[1] Notice that the values of the angular velocity reported in these figures are those measured in the rotating frame of reference. Values in the non-rotating frame of reference are simply obtained as $(\omega_{in}/\Omega)_{nr\text{-}frame} = \omega_{in}/\Omega + 1$.

and an intrinsic increase of the number of stars on retrograde orbits (which may be easily interpreted in light of an argument based on the conservation of angular momentum), initially non-rotating clusters acquire an approximately solid-body retrograde rotation in their outermost regions with angular velocity $\omega/\Omega \approx -0.5$. In this section, we show that this effect also applies to the outer regions of the rotating models considered in this paper.

Fig. 1 shows that the systems we have explored here have already acquired an outer retrograde rotation early during the violent relaxation phase (see also Vesperini et al. 2014). In order to provide a more detailed characterization of the distribution of angular momentum in the outer regions, we have measured the slope of the rotation curve (calculated in the rotating frame of reference described in Section 2) for particles at radii $R > 0.5r_J$. Hereafter, we refer to this slope as ω_{out}, and Figs 13 and 14 show the evolution of ω_{out}/Ω as a function of time (normalized to the initial half-mass relaxation time) and the fraction of the initial mass remaining in the cluster.

The model with the larger initial ratio of the half-mass to Jacobi radius, r_h/r_J, (vrQ01F05), starts its evolution with a value ω_{out}/Ω approximately equal to -0.5 acquired during the violent relaxation phase and retains this value for the entire simulation. The two models with smaller initial values of r_h/r_J (vrQ01F02 and vrQ001F05) emerge from the violent relaxation phase with ω_{out}/Ω approximately equal to -1, but after losing a small amount of mass, their outer angular velocities converge to values close to -0.5 for the rest of the simulation.

4 CONCLUSIONS

In this paper, we have presented the results of a survey of *N*-body simulations aimed at exploring the long-term evolution of rotation in star clusters evolving in the tidal field of the host galaxy. All models acquire a differential rotation during their early evolution while they undergo a phase of violent relaxation; their rotation curves are characterized by a shape rising from the centre of the cluster, peaking at approximately 1–2 half-mass radii, then decreasing in the outer regions and becoming slightly retrograde in the outermost regions.

We first discussed the evolution of the entire rotation curve of each of the models (Section 3.1; Figs 1–3) and then focused our attention on the properties of the rotation curve in the cluster innermost (Section 3.3) and outermost (Section 3.4) regions as well as on the strength and location of the peak of the rotational velocity (Section 3.2).

Our simulations show that as a result of the transport of angular momentum from the inner to the outer regions and star escape carrying away angular momentum, the peak of the rotation curve and the slope of the rising inner part of the rotation curve decrease as the cluster evolves and lose stars. For all the models we have explored, the peak of the rotational velocity and the inner angular velocity normalized to their initial values have an approximately universal dependence on the fraction of the initial mass remaining in the cluster (see Figs 5 and 11). We find that even after losing a significant fraction of their initial mass, clusters can retain some of their initial rotation.

We have quantified the relative strength of the ordered rotational motion to the random thermal motion by studying the evolution of the peak of the rotational velocity normalized to the central velocity dispersion v_{pk}/σ_0, as often done in observational studies, as well as the evolution of the peak of the ratio of the rotational velocity profile to the velocity dispersion profile, $(v_\phi/\sigma)_{pk}$. As the cluster
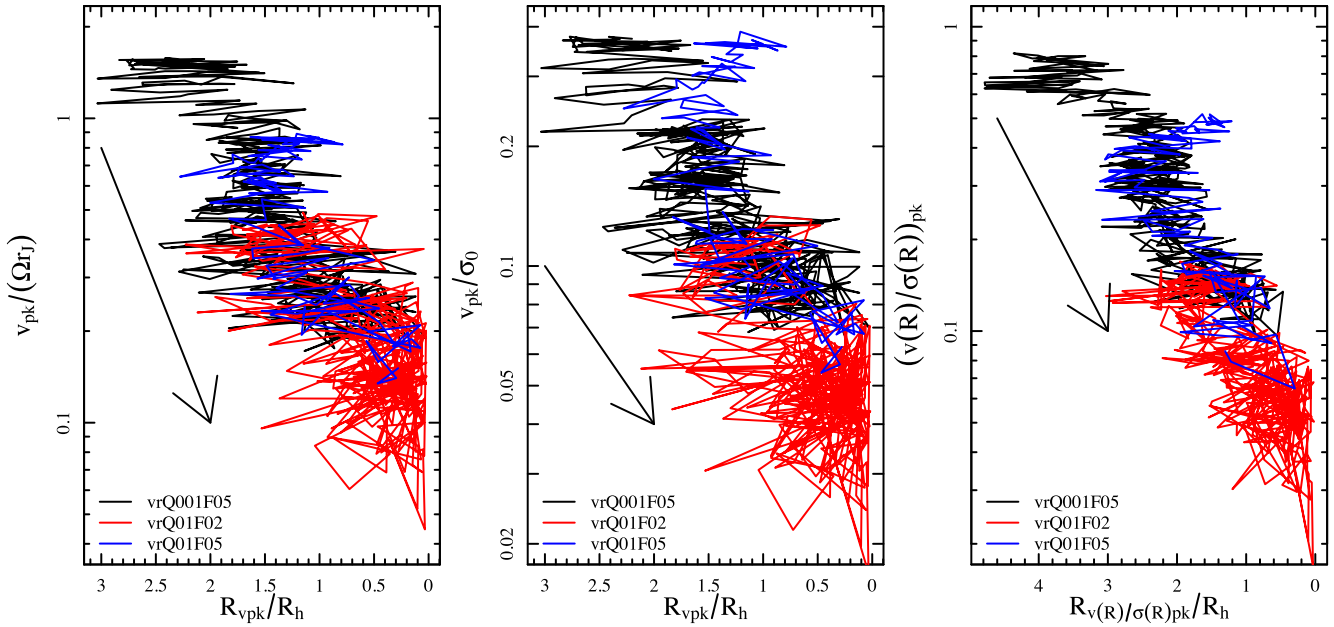
Figure 9. Left-hand panel: evolution of the magnitude of the peak of the rotation curve, normalized to Ω times the current Jacobi radius, as a function of its location at that time. Middle panel: evolution of v_{pk}/σ_0 as a function of its location at that time. Right-hand panel: evolution of the peak of the v_ϕ/σ profile as a function of its location at that time. The arrows show the direction of evolution.
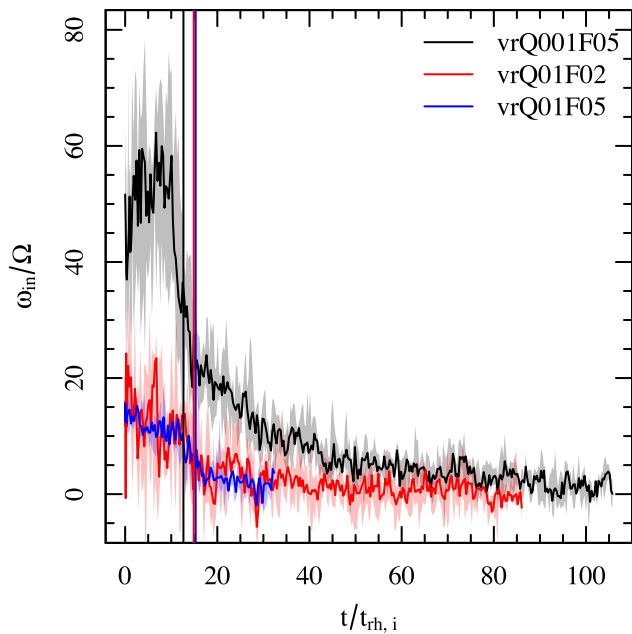
Figure 10. Evolution of the slope of the rotation curve between 0.1 and $0.5R_h$ for all the simulations. Time is normalized to the initial half-mass relaxation time, while the slope is normalized to the cluster's orbital angular velocity. The shaded areas represent the range covered by the four realizations for each model, and the vertical lines mark the median time of core collapse.

Figure 11. Evolution of ω_{in}, normalized to its initial value as a function of fraction of initial mass remaining.

evolves and loses part of its initial angular momentum, it becomes increasingly dominated by random motions, but even after several tens of initial relaxation times, a cluster can still be characterized by non-negligible values of v_{pk}/σ_0 and $(v_\phi/\sigma)_{pk}$. In all cases, our simulations show that the current rotation observed in clusters provides only a lower limit on the strength of initial rotation, and thus small current values of rotation should not be taken as an indication
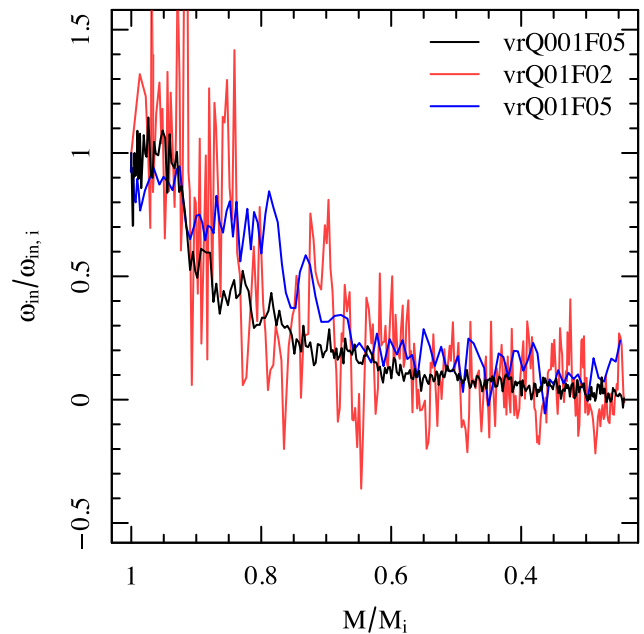
of the lack of importance of rotation in the past dynamical history of star clusters.

We have explored the evolution of the location of the peak, R_{pk}, of the rotation curve over time and found this to be located for most of the cluster evolution between 1 and $2R_h$, although it gradually evolves towards the cluster inner regions, and in the late phases of cluster evolution, it can be found at $R_{pk}/R_h \sim 0.5$–1.

As for the rotation in the cluster outermost regions, we have shown that all models evolve towards an approximately solid-body retrograde rotation with angular velocity approximately equal to
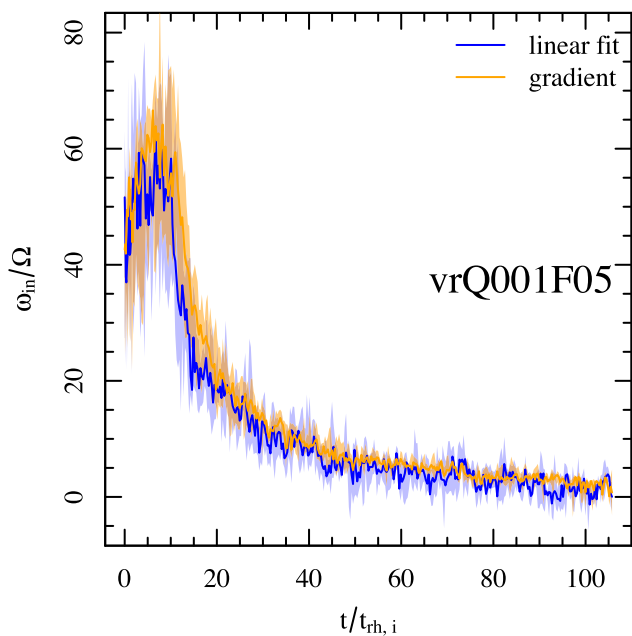
Figure 12. $\omega_{\rm in}/\Omega$ versus $t/t_{\rm rh,\,i}$ using the two different methods described in Section 3.3. The shaded areas represent the range covered by the four realizations.
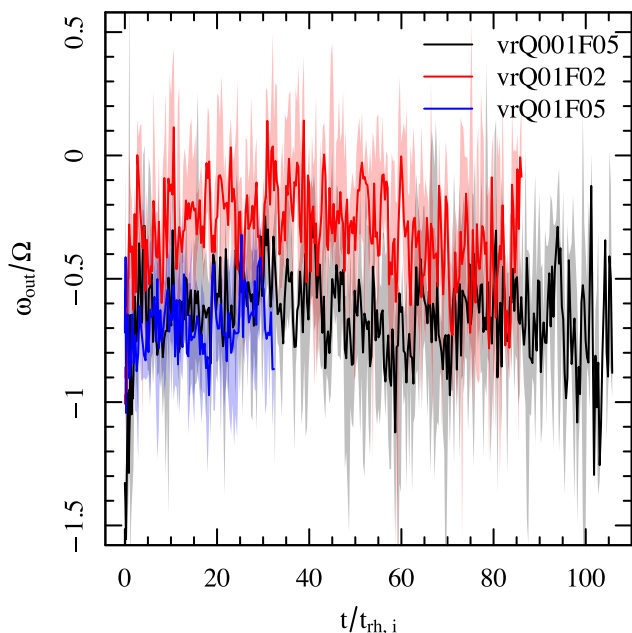

Figure 13. Time evolution of the slope of rotation curve in the outermost regions ($R > 0.5r_{\rm J}$) of the cluster for all models. The shaded areas represent the range covered by the four realizations for each model.

half of the orbital angular velocity, in agreement with what found in our previous study for a set of initially non-rotating models (Tiongco et al. 2016b).

In a forthcoming paper, we will continue our investigation of the interplay between internal rotation and the effects of an external tidal field by further extending our investigation of the role of different structural and kinematical parameters in the evolution of the angular momentum of star clusters. Specifically, we will explore the long-term dynamical evolution of the kinematical and morphological properties, in the presence of a tidal perturbation, of a general
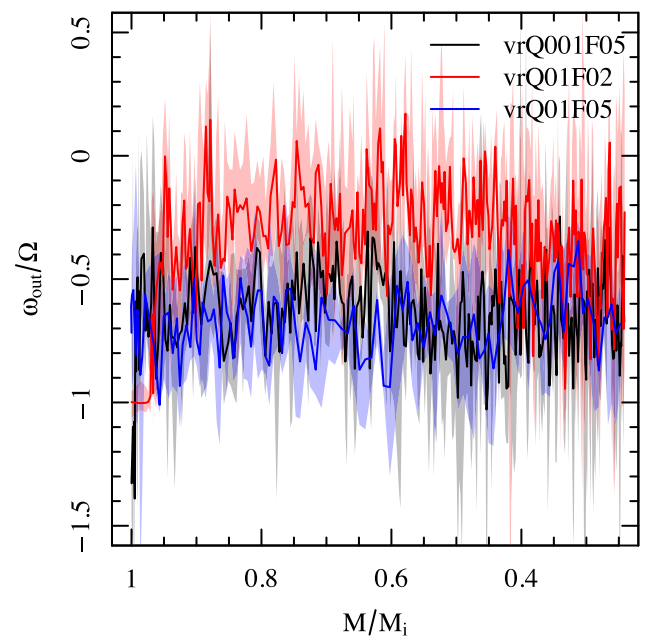

Figure 14. Similar to Fig. 13, but as a function of fraction of mass remaining in the cluster.

class of rotating systems sampled from the family of distribution-function-based models introduced by Varri & Bertin (2012).

REFERENCES

Aarseth S. J., 2003, Gravitational N-Body Simulations. Cambridge Univ. Press, Cambridge
Akiyama K., Sugimoto D., 1989, PASJ, 41, 991
Bellazzini M., Bragaglia A., Carretta E., Gratton R. G., Lucatello S., Catanzaro G., Leone F., 2012, A&A, 538, A18
Bellini A. et al., 2015, ApJ, 810, L13
Bianchini P., Varri A. L., Bertin G., Zocchi A., 2013, ApJ, 772, 67
Chen C. W., Chen W. P., 2010, ApJ, 721, 1790
Cordero M. J., Hénault-Brunet V., Pilachowski C. A., Balbinot E., Johnson C. I., Varri A. L., 2017, MNRAS, 465, 3515
Einsel C., Spurzem R., 1999, MNRAS, 302, 81
Ernst A., Glaschke P., Fiestas J., Just A., Spurzem R., 2007, MNRAS, 377, 465
Fabricius M. H. et al., 2014, ApJ, 787, L26
Giersz M., Heggie D. C., 1994, MNRAS, 270, 298
Heggie D., Hut P., 2003, The Gravitational Million-Body Problem: A Multidisciplinary Approach to Star Cluster Dynamics. Cambridge Univ. Press, Cambridge
Hénault-Brunet V. et al., 2012, A&A, 546, A73
Hong J., Kim E., Lee H. M., Spurzem R., 2013, MNRAS, 430, 2960
Inagaki S., Hachisu I., 1978, PASJ, 30, 39
Kacharov N. et al., 2014, A&A, 567, A69

Kim E., Einsel C., Lee H. M., Spurzem R., Lee M. G., 2002, MNRAS, 334, 310

Kim E., Lee H. M., Spurzem R., 2004, MNRAS, 351, 220

Kim E., Yoon I., Lee H. M., Spurzem R., 2008, MNRAS, 383, 2

King I. R., 1966, AJ, 71, 64

Lane R. R., Kiss L. L., Lewis G. F., Ibata R. A., Siebert A., Bedding T. R., Székely P., Szabó G. M., 2011, A&A, 530, A31

Lardo C. et al., 2015, A&A, 573, A115

McLaughlin D. E., van der Marel R. P., 2005, ApJS, 161, 304

Mapelli M., 2017, MNRAS, 467, 3255

Meylan G., Heggie D. C., 1997, A&AR, 8, 1

Miocchi P. et al., 2013, ApJ, 774, 151

Nitadori K., Aarseth S. J., 2012, MNRAS, 424, 545

Richer H. B., Heyl J., Anderson J., Kalirai J. S., Shara M. M., Dotter A., Fahlman G. G., Rich R. M., 2013, ApJ, 771, L15

Spitzer L., 1987, Dynamical Evolution of Globular Clusters. Princeton Univ. Press, Princeton, NJ

Tiongco M. A., Vesperini E., Varri A. L., 2016a, MNRAS, 455, 3693

Tiongco M. A., Vesperini E., Varri A. L., 2016b, MNRAS, 461, 402

Varri A. L., Bertin G., 2012, A&A, 540, A94

Vesperini E., Varri A. L., McMillan S. L. W., Zepf S. E., 2014, MNRAS, 443, L79

Watkins L. L., van der Marel R. P., Bellini A., Anderson J., 2015, ApJ, 803, 29

White R. E., Shawl S. J., 1987, ApJ, 317, 246

Wilson C. P., 1975, AJ, 80, 175

This paper has been typeset from a TEX/LATEX file prepared by the author.